ELSEVIER

Journal of Wind Engineering
and Industrial Aerodynamics 91 (2003) 309–329

JOURNAL OF wind engineering AND industrial aerodynamics

www.elsevier.com/locate/jweia

Effects of inflow turbulence intensity on flow and pollutant dispersion in an urban street canyon

Jae-Jin Kim[a,1], Jong-Jin Baik[b,*]

[a] *Department of Environmental Science and Engineering, Kwangju Institute of Science and Technology, Gwangju 500-712, South Korea*

[b] *School of Earth and Environmental Sciences, Seoul National University, Seoul 151-742, South Korea*

Received 24 June 2001; received in revised form 1 March 2002; accepted 17 July 2002

Abstract

The effects of inflow turbulence intensity on flow and pollutant dispersion in an urban street canyon with a street aspect ratio of 1 are examined using a two-dimensional numerical model. As the inflow turbulence intensity increases, turbulent kinetic energy and turbulent diffusivity in the street canyon increases. Also, the mean horizontal velocity near the roof level increases and the street-canyon vortex strengthens. The analyses of the time series and residue ratio of pollutant concentration show that the inflow turbulence intensity significantly affects pollutant concentration in the street canyon. As the inflow turbulence intensity increases, the pollutant concentration in the street canyon becomes low and hence more pollutants escape from the street canyon.

Keywords: Inflow turbulence intensity; Urban street-canyon flow; Pollutant dispersion; Turbulent kinetic energy; Turbulent diffusivity

1. Introduction

Harmful pollutants emitted from traffic vehicles in an urban area cause severe damage to human being and their property. In order to minimize potential damage occurring inevitably due to human activity, it is demanded not only to reduce emission of harmful pollutants but also to understand and accurately predict urban

*Corresponding author. Tel.: +82-2-880-6990; fax: +82-2-883-4972.
E-mail address: jjbaik@snu.ac.kr (J.-J. Baik).
[1] Present address: Environmental Fluid Dynamics Program, Department of Mechanical and Aerospace Engineering, Arizona State University, USA.

0167-6105/03/$ - see front matter
PII: S0167-6105(02)00395-1

flow and pollutant dispersion. An urban street canyon is a space surrounded by a city road and its flanking buildings and a main pollutant-emitting source, traffic vehicles, is located at the street. Therefore, a study of flow and pollutant dispersion in an urban street canyon should be a first step to understand complex urban flow and dispersion.

Meteorological conditions such as ambient wind speed and direction, atmospheric stability, and solar radiation influence urban street-canyon flow. The ambient wind speed determines vortex generation [1] and its intensity [2]. It also determines retention time of pollutants emitted into a street canyon [3,4]. In order to generate and maintain vortices in a street canyon, the ambient wind speed should exceed a certain critical value. However, even if the ambient wind speed exceeds a certain critical value, the vortex generation and maintenance can still depend on ambient wind direction. This explains the importance of the ambient wind direction to the concentration distribution of passive pollutants [5–7]. For a street canyon formed by different building heights, the ambient wind direction plays an important role in determining vortex number and flow field in the street canyon [6,8]. The atmospheric stability affects street-canyon flow. The street-canyon vortex tends to be weak when the atmosphere is stable and strong when unstable [9]. When the street bottom or building wall is heated by solar radiation, thermally induced flow is formed in the canyon. This thermally induced flow is combined with mechanically induced flow formed in the canyon when there is no solar heating, producing interesting flow patterns, depending on street aspect ratio and the degree of heating [10,11].

When wind blows over buildings with different shapes and sizes, it is disturbed by the buildings and mechanically produced turbulent eddies can stream into a street canyon. That is, for a street canyon, the inflow turbulence intensity can vary, depending on the geometric configuration of the surrounding buildings [12]. The field data by Kato et al. [13] reveal that the ambient turbulence intensity can vary significantly even if the ambient flow speed remains the same. Zhang et al. [14] investigated the effects of inflow turbulence level on the recirculation zone generated behind an isolated cubical obstacle by including or excluding turbulent diffusion term. They found that the inflow turbulence reduces the size of the recirculation zone. In spite of dynamical importance of surrounding turbulence level affecting urban street-canyon flow, there is, to our knowledge, no systematic study investigating it.

In this study, the effects of inflow turbulence intensity on flow and pollutant dispersion in a street canyon are examined in a dynamical viewpoint. For this, mean flow, turbulence, and mean pollutant concentration fields simulated with various inflow turbulence intensities are analyzed and dynamical process involved is searched.

2. The numerical model

The numerical model used in this study is the same as that of [2], which employs a two-dimensional, nonhydrostatic, nonrotating, incompressible airflow system. The

turbulence parameterization in the numerical model is described in the appendix. For other details of the numerical model, see [2]. Fig. 1 shows model domain configuration. Both horizontal and vertical domain sizes are 100 m and the grid interval is 1 m in both directions. The time step is 0.05 s. The building height is 40 m and the width between the upwind and downwind buildings is also 40 m. Therefore, the street aspect ratio, defined as the ratio of the building height to the street width, is one. One hundred numerical experiments are performed with different values of turbulent kinetic energy (TKE) at the inflow boundary. Inflow boundary conditions for model variables are listed in Table 1. At the outflow and upper boundaries, the gradient of any variable is set to zero. In this study, it is considered that a level of TKE represents turbulence intensity and the inflow turbulence is advected through the inflow boundary. The inflow turbulence intensity is given by the ratio of the inflow TKE to the inflow mean kinetic energy. In the case of TI1, the inflow TKE is

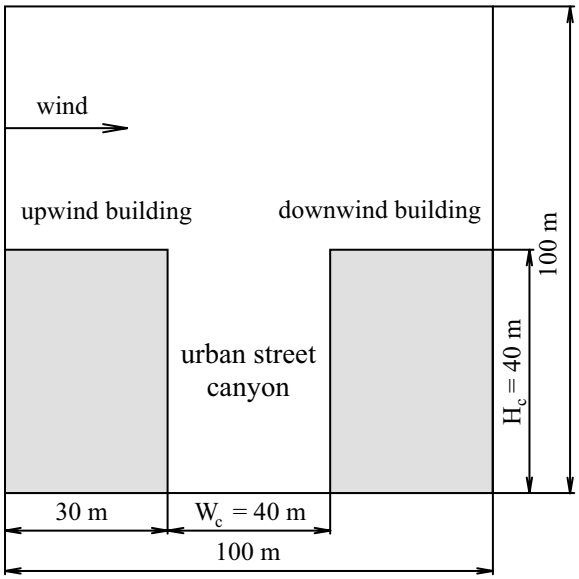

Fig. 1. Model domain configuration for this study.

Table 1
Inflow boundary conditions for numerical experiments with different inflow turbulence intensities

Aspect ratio	$H_c/W_c = 1$
Horizontal velocity	$U_0 = 2.5(z/z_r)^{0.299}$
Vertical velocity	$W_0 = 0$
Turbulent kinetic energy	$k_0 = 0.001nU_0^2$, $n = 1, 2, \ldots, 100$ (denoted by TI1, TI2,…, TI100 cases)
Dissipation	$\varepsilon_0 = C_\mu^{3/4} k_0^{3/2}/\kappa z$

Here, z is the height, $z_r = 10$ m, C_μ is a constant (=0.09), and κ is the von Karman constant.

0.2% of the inflow mean kinetic energy. In the cases of TI2–TI100, the inflow TKE increases with an increment of 0.2%.

The numerical model is firstly integrated up to $t = 1$ h for flow fields and then the conservation equation for passive pollutants is integrated for 1 h using flow fields at $t = 1$ h. There are 40 point sources at the street bottom and each point source emits passive pollutants at a rate of $5\,\text{ppb}\,\text{s}^{-1}$.

3. Results and discussion

3.1. Inflow turbulence intensity effects on flow

Fig. 2 shows streamline fields in the cases of TI20, TI40, TI60, and TI80, which are plotted using mean velocity fields. Despite different inflow turbulence intensities, the patterns of streamline field are very similar to each other. In all the cases, one vortex is formed in the canyon with a street aspect ratio of 1 and the vortex center is located above and downstream of the canyon center ($x = 50$ m, $z = 20$ m).

Fig. 3 shows the vertical profiles of TKE and horizontal velocity at $x = 15$, 35, 50, 65, and 85 m above $z = 40$ m (canyon-top height or roof level) in the cases of TI20

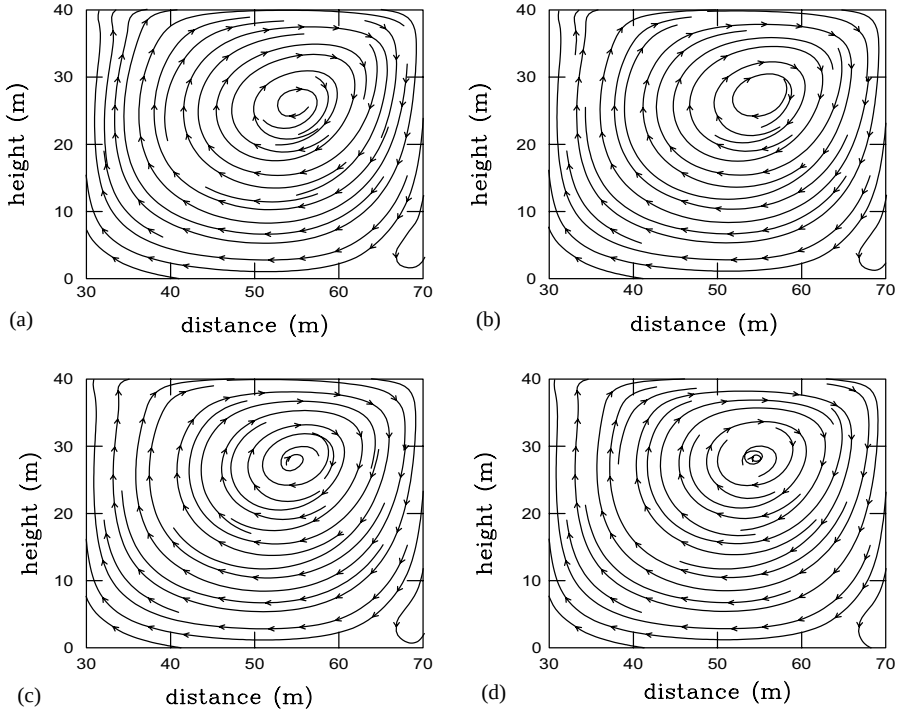

Fig. 2. Streamline fields at $t = 1$ h in the (a) TI20, (b) TI40, (c) TI60, and (d) TI80 cases.

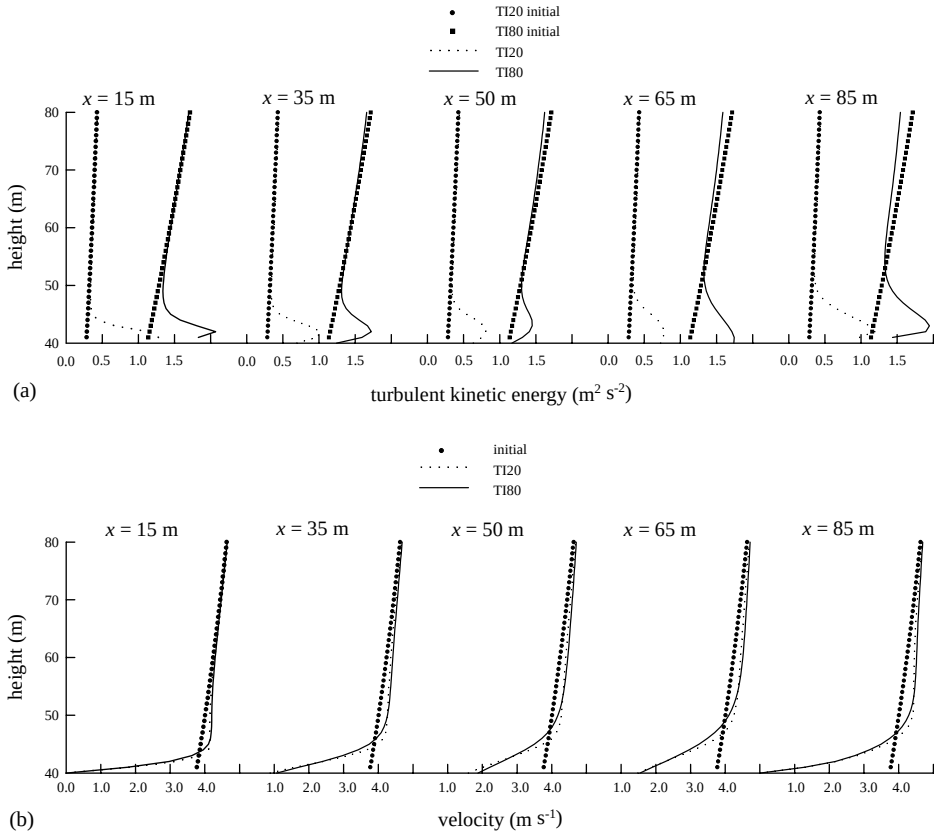

Fig. 3. The vertical profiles of (a) turbulent kinetic energy and (b) horizontal velocity at $x = 15$ m, 35 m (near the upwind building), $x = 50$ m (at the center of the street canyon), $x = 65$ m (near the downwind building), and $x = 85$ m above $z = 40$ m at $t = 1$ h in the TI20 and TI80 cases.

and TI80. As the inflow turbulence intensity increases, TKE at all the locations increases. It should be noticed that horizontal and vertical velocities and pollutant concentration presented in this study are the Reynolds-averaged mean quantities. At the upwind-building location, the vertical profile of TKE in the region above $z \sim 48$ m is essentially the same as that at the inflow boundary (Fig. 3a). Near the roof level ($\sim 40\,\text{m} < z < \sim 45\,\text{m}$), there is a layer with high TKE. This is consistent with the results from wind-tunnel experiment [15], numerical modeling [16], and field observation [17]. The high-TKE layer deepens across the street canyon. The maximum value of TKE near the roof level decreases as one passes the central and upwind regions of the street canyon but increases again near the downwind building.

In order to examine why the high TKE is observed above the roof level, the TKE budget analysis was performed at $z = 41$ m in the TI10 case. Results showed that shear production term is larger than any other terms at most locations. Near the roof level, the vertical shear of horizontal wind is very strong (Fig. 3b). TKE production

by wind shear was maximum near the downwind building edge because the horizontal gradient of vertical wind as well as the vertical gradient of horizontal wind is very large there. These results are the same as those of [2].

The $k-\varepsilon$ type turbulence closure schemes have been successfully used in numerous engineering problems. The present model also employs a $k-\varepsilon$ turbulence closure scheme to represent turbulent processes (see the appendix). The present model was verified against wind-tunnel data [18], showing that the model simulates mean flow and pollutant concentration reasonably well. It is, however, known that turbulence fields simulated using $k-\varepsilon$ closure schemes deviate from experimental data to some degree depending on which turbulence scheme is used, although mean flow fields are well simulated. The present model is not yet verified against experimental TKE data, requiring further research on the verification of TKE field in a street canyon and thereby the improvement of the present $k-\varepsilon$ scheme.

Above the upwind building, downward momentum transfer is prevented by the presence of the building. As a result, momentum transferred from the upper layer is accumulated near the roof level ($z > \sim 44$ m) and the horizontal velocity increases there (Fig. 3b). Above the upwind building, the increase of horizontal velocity is confined to a certain vertical region. As flow passes over the upwind building and enters above-canyon region, momentum starts to be transferred into the street canyon. Accordingly, the horizontal velocity at the roof level increases but its vertical shear decreases. However, the horizontal velocity at the roof level decreases near the downwind building. Fig. 3b shows that the horizontal velocity above the roof level increases or decreases with height as the inflow turbulence intensity increases.

This increase or decrease of horizontal velocity with height can be understood with the degree of momentum transfer. Fig. 4 shows a sketch for the horizontal velocity change with height when the inflow turbulence intensity is relatively low/high, based on the simulation results. Above the upwind building, momentum transferred from the L1 layer is accumulated and the horizontal velocity increases. Momentum transfer into the L2 layer increases because turbulent diffusivity increases with increasing inflow turbulence intensity. Therefore, the horizontal velocity increases but its vertical shear decreases with increasing inflow turbulence intensity in the L1 layer. Near the roof level, TKE is relatively high compared with that at other levels because of its vigorous production by the strong wind shear and increases with increasing inflow turbulence intensity. Consequently, the increase of turbulent diffusivity in the L2 layer makes the vertical shear of horizontal velocity decrease. As momentum starts to be transferred into the street canyon, a variation in the velocity profile is much pronounced. The increase of turbulent diffusivity resulting from the increase of inflow turbulence intensity enhances momentum transfer into the street canyon and the horizontal velocity at the roof level increases. In the L2 layer, the decrease in the vertical shear of horizontal velocity becomes large. Accordingly, the horizontal velocity decreases in the middle region of the L2 layer but increases in the L1 layer and the upper and lower regions of the L2 layer.

Fig. 5 shows the distributions of TKE in the cases of TI20, TI40, TI60, and TI80. As the inflow turbulence intensity increases, TKE in the street canyon increases.

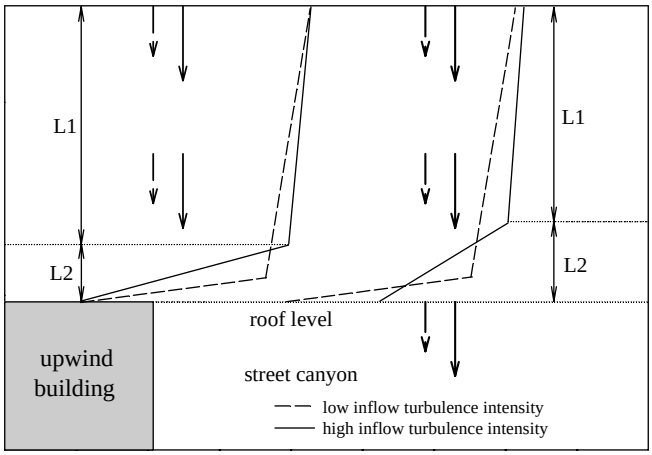

Fig. 4. A sketch for the horizontal velocity change with height above the upwind building and street canyon when the inflow turbulence intensity is relatively low/high. The arrows denote the downward momentum transfer.

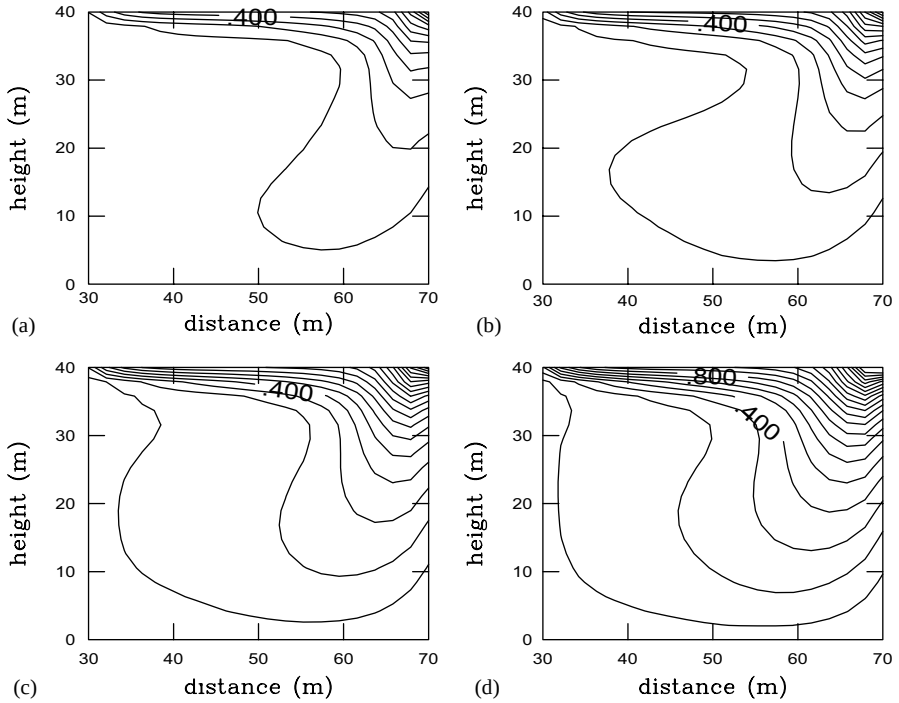

Fig. 5. Turbulent kinetic energy fields at $t = 1$ h in the (a) TI20, (b) TI40, (c) TI60, and (d) TI80 cases. The contour interval is $0.1\,m^2\,s^{-2}$.

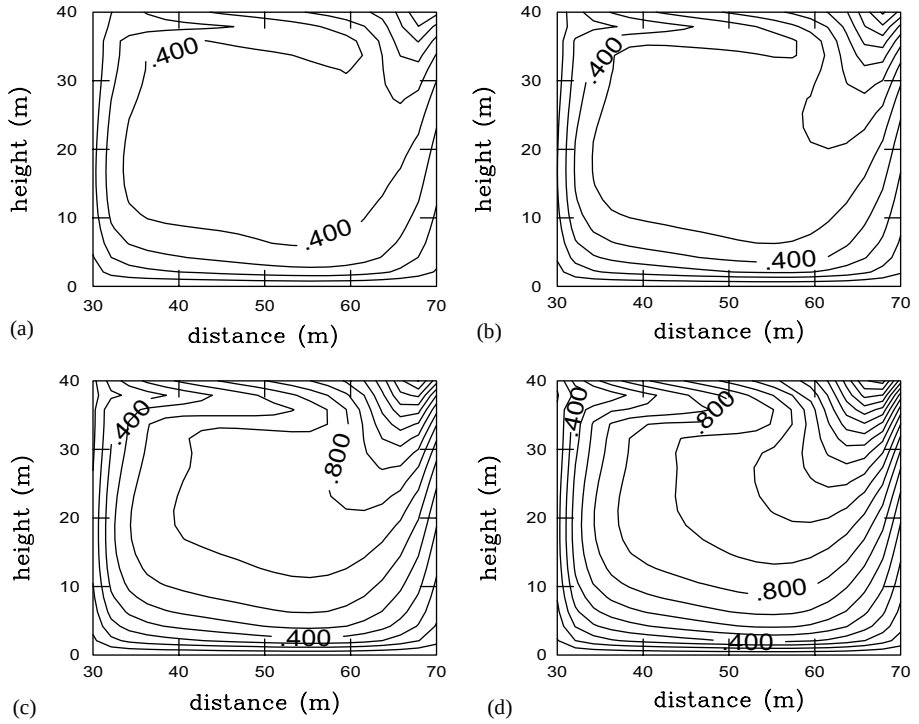

Fig. 6. Same as Fig. 5 except for turbulent diffusivity of momentum. The contour interval is $0.1\,m^2\,s^{-1}$.

TKE is high near the roof level and downwind region of the street canyon. This figure indicates that high TKE near the roof level is advected into the street canyon mainly in the downwind region.

Fig. 6 shows turbulent momentum diffusivity distributions corresponding to the cases in Fig. 5. Turbulent diffusivity in the street canyon increases with increasing inflow turbulence intensity. Beneath the roof level, turbulent diffusivity is smaller in the upwind region than near the downwind building. When the inflow turbulence intensity is relatively weak (Figs. 6a and b), very high turbulent diffusivity is observed just at the roof level near the downwind building and relatively low turbulent diffusivity is distributed roughly symmetrically in the street canyon. When the inflow turbulence intensity is relatively strong (Figs. 6c and d), very high turbulent diffusivity permeates into the street canyon. Hence, relatively high turbulent diffusivity appears as going to the street-canyon center region from the downwind region and symmetric distribution pattern is broken. The increase of turbulent diffusivity contributes to an even distribution of momentum.

Fig. 7 shows maximum and minimum horizontal and vertical velocities and TKE in the street canyon as a function of inflow turbulence intensity. As the inflow turbulence intensity increases, the maximum streamwise horizontal velocity (horizontal flow toward the right) increases because momentum transfer from the

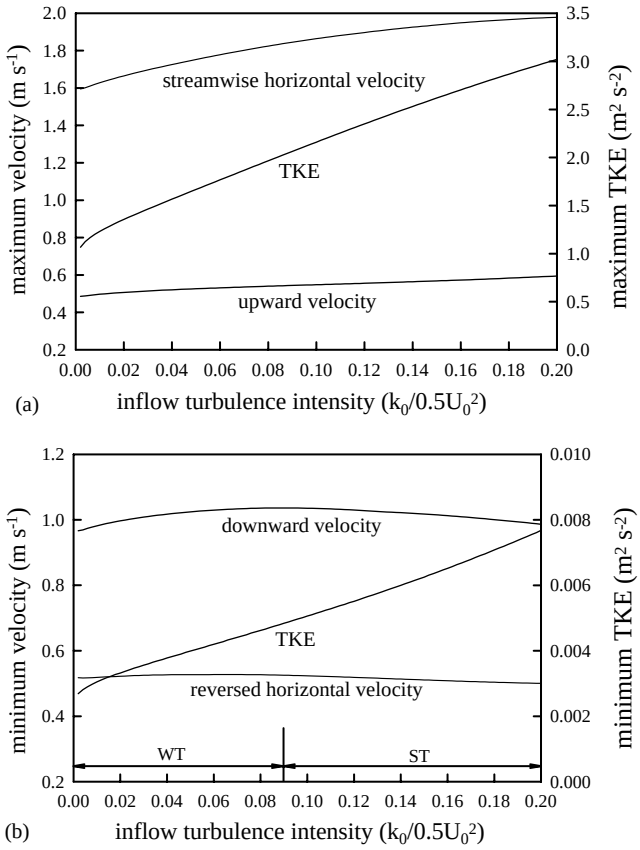

Fig. 7. (a) Maximum streamwise horizontal and upward velocities and turbulence kinetic energy and (b) maximum reversed horizontal and downward velocities and minimum turbulent kinetic energy as a function of inflow turbulence intensity in the street canyon.

above-canyon region into the street canyon increases. Also, the maximum upward velocity increases with increasing inflow turbulence intensity but its increasing rate is small. The reversed horizontal velocity (horizontal flow toward the left) and downward velocity do not exhibit a monotonous variation with inflow turbulence intensity. It might be convenient to categorize simulated cases based on the variation of the downward velocity, although the variation with inflow turbulence intensity is very small. The first category appears when the inflow turbulence intensity is relatively weak (hereafter, WT). In this category (TI1–TI45), the maximum downward velocity slightly increases with increasing inflow turbulence intensity. The second category appears when the inflow turbulence intensity is relatively strong (ST). In this category (TI46–TI100), the maximum downward velocity slightly decreases as the inflow turbulence intensity increases due to strong turbulent mixing.

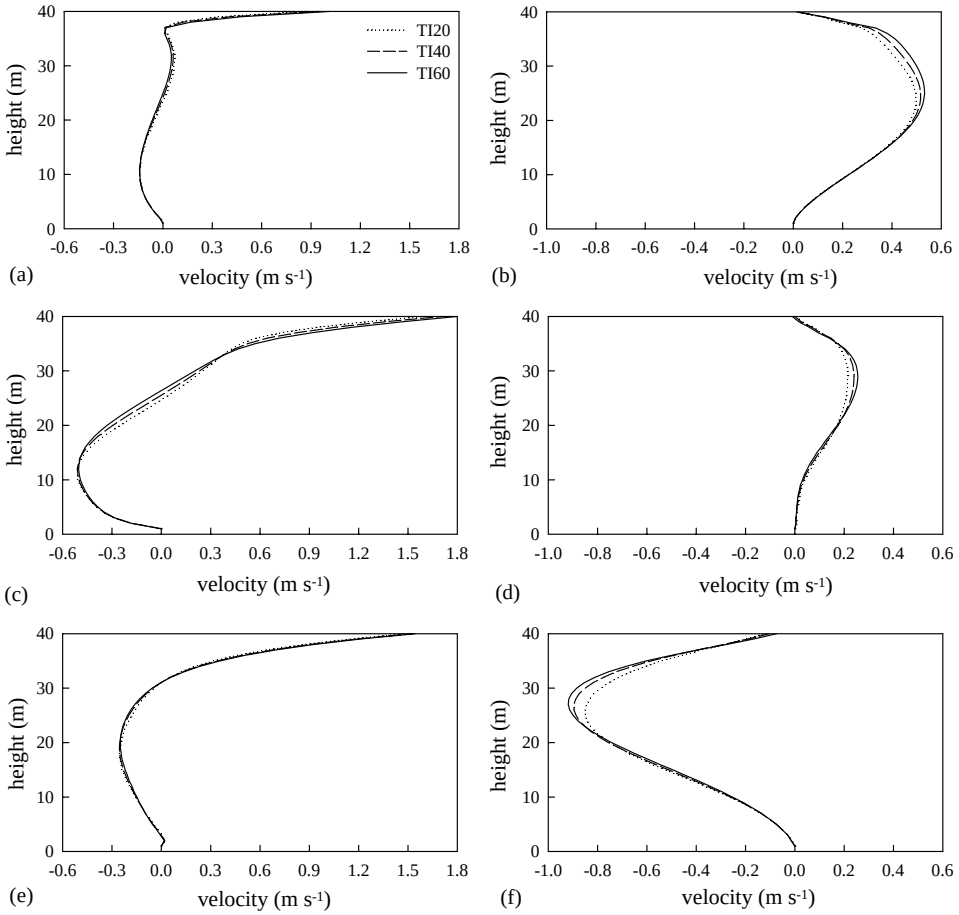

Fig. 8. The vertical profiles of horizontal (left) and vertical (right) velocities at $x = 35$ m [(a) and (b)], $x = 50$ m [(c) and (d)], and $x = 65$ m [(e) and (f)] at $t = 1$ h in the TI20, TI40, and TI60 cases.

The maximum streamwise velocity in the street canyon is observed at the roof level. The height where the maximum reversed velocity is observed tends to increase with increasing inflow turbulence intensity ($z = 11$ m in the TI1 case, $z = 14$ m in the TI100 case). The maximum upward velocity is observed at $x = 37$ or 38 m in all the cases but its height tends to increase with increasing inflow turbulence intensity ($z = 23$ m in the TI1 case, $z = 27$ m in the TI100 case). The maximum downward velocity is observed at a nearly fixed location near the downwind building ($x = 67$ or 68 m, $z = 29$ or 30 m) in all the cases.

Fig. 8 shows the vertical profiles of horizontal and vertical velocities at $x = 35$, 50, and 65 m in the TI20, TI40, and TI60 cases. Within a few meters beneath the roof level, the horizontal velocity increases with increasing inflow turbulence intensity. This results from the increase of momentum transfer from the ambient flow (Fig. 4).

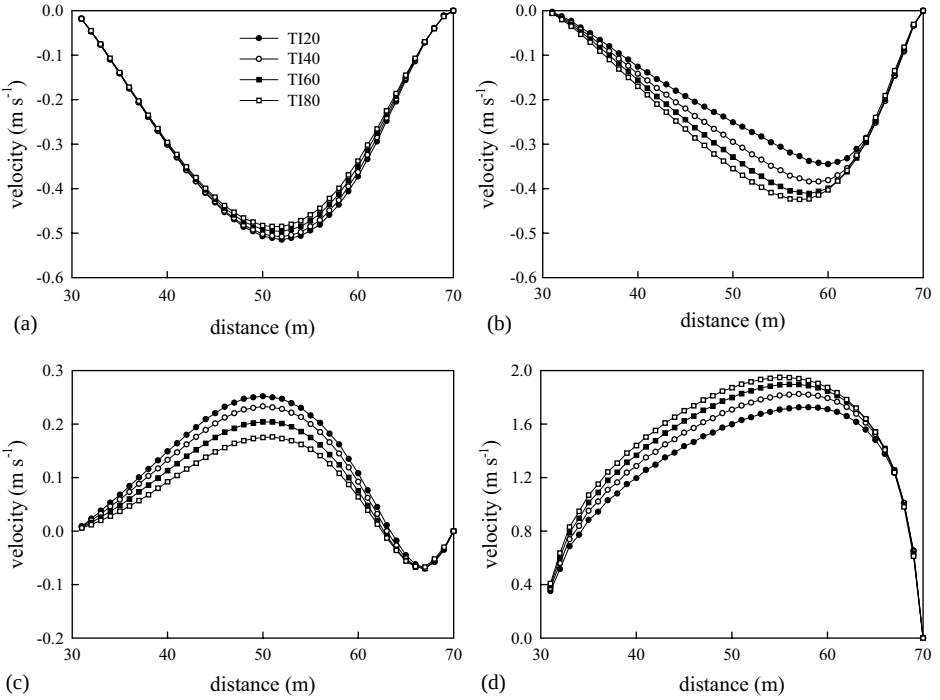

Fig. 9. The horizontal distributions of horizontal velocity at (a) $z = 10$ m, (b) $z = 20$ m, (c) $z = 30$ m, and (d) $z = 40$ m at $t = 1$ h in the TI20, TI40, TI60, and TI80 cases.

In the lower layer, the reversed horizontal velocity rather weakens despite the increase of momentum transfer. This is not only because the region of reversed horizontal velocity widens but also because the increased turbulent diffusivity distributes reversed horizontal velocity more evenly and decreases its peak. The vertical profiles of horizontal velocity at the street-canyon center (Fig. 8c) indicate that the vortex-center height increases as the inflow turbulence intensity increases. The small but complicated variations of the vertical profiles with inflow turbulence intensity are considered to result from both the vortex-center rise and the momentum redistribution due to the increase of turbulent diffusivity. As the inflow turbulence intensity increases, the magnitude of vertical velocity decreases slightly in the lower layer but increases in the upper layer (Figs. 8b, d, and f). The heights of maximum upward and downward velocities at each location increase with increasing inflow turbulence intensity. This is largely because the height of vortex center increases as the inflow turbulence intensity increases (Fig. 2). However, note that the maximum downward velocity in the street canyon is observed at a nearly fixed height ($z = 29$ or 30 m).

Fig. 9 shows the horizontal distributions of horizontal velocity at $z = 10$, 20, 30, and 40 m in the TI20, TI40, TI60, and TI80 cases. As the inflow turbulence intensity

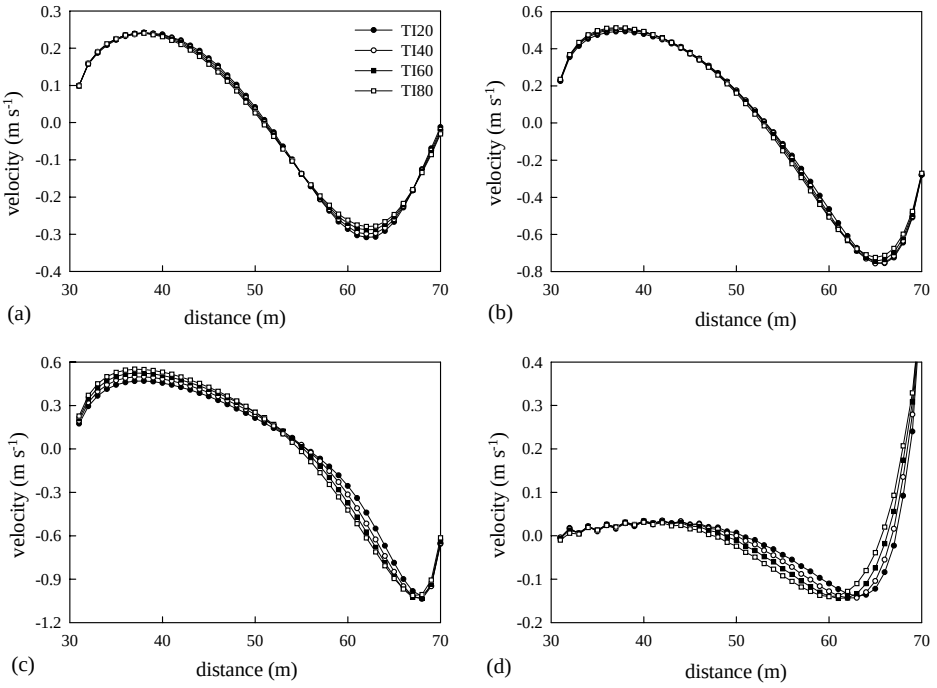

Fig. 10. Same as Fig. 9 except for vertical velocity.

increases, the reversed horizontal velocity decreases at $z = 10\,\mathrm{m}$ but increases at $z = 20\,\mathrm{m}$. At $z = 30\,\mathrm{m}$, the streamwise horizontal velocity in the region of $30\,\mathrm{m} < x < 63\,\mathrm{m}$ decreases but the reversed horizontal velocity near the downwind building increases. At the roof level, the streamwise horizontal velocity increases and its peak location shifts toward the street center with increasing turbulence intensity. The increase of streamwise horizontal velocity is larger in the upwind region than in the downwind region.

Fig. 10 shows the corresponding vertical velocity distributions. At $z = 10\,\mathrm{m}$, as a whole, both upward and downward velocities decrease with increasing inflow turbulence intensity. At $z = 20\,\mathrm{m}$, except for the region near the downwind building ($\sim 63\,\mathrm{m} < x < \sim 70\,\mathrm{m}$), the upward and downward velocities slightly increase with increasing inflow turbulence intensity. At $z = 30\,\mathrm{m}$, the variation trend of vertical velocity is similar to that at $z = 20\,\mathrm{m}$. As the inflow turbulence intensity increases, the maximum downward velocity near the downwind building increases when the inflow turbulence intensity is relatively weak (TI20 and TI40 cases) but decreases when the inflow turbulence intensity is relatively strong (TI60 and TI80 cases). These are typical characteristics of the WT and ST cases. Note that in the ST cases, the maximum downward velocity near the downwind building decreases but the vertical motion becomes strong at most locations except for near the downwind building. At the roof level, there is little variation in the upward velocity in the upwind region but

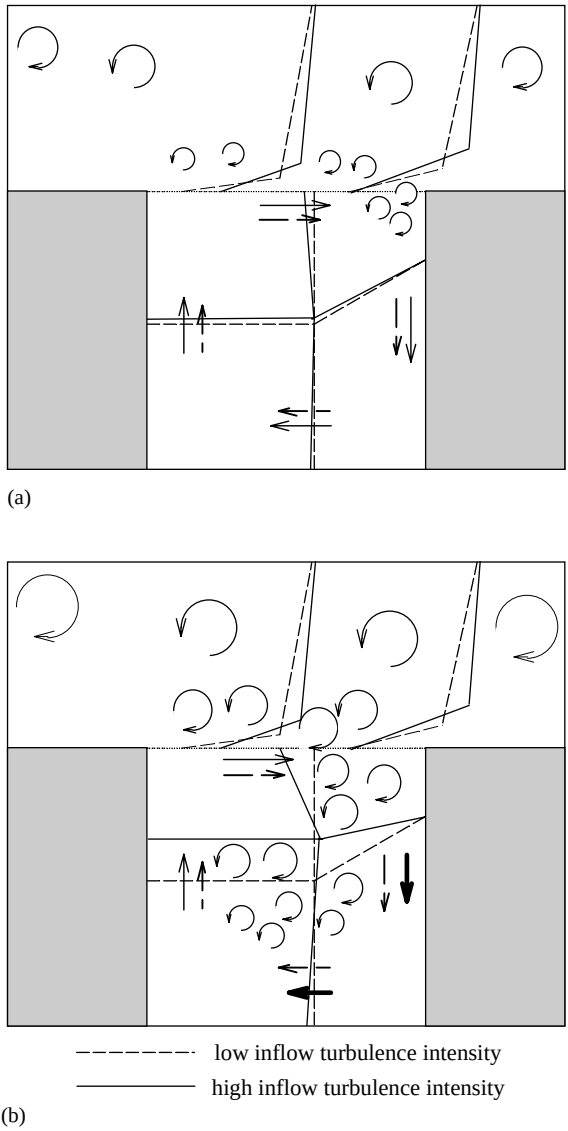

Fig. 11. Sketches for explaining flow changes with inflow turbulence intensity in the (a) WT and (b) ST cases. The sizes of turbulent eddies are exaggerated for explanation.

much variation in the downward velocity in the downwind region. Downward motion appears at a farther upwind location and in a wider area as the inflow turbulence intensity increases. This is considered to cause enhanced advection of high TKE near the roof level into the street canyon.

Based on the analysis results presented above, Figs. 11a and b are drawn, which schematically explain flow changes with inflow turbulence intensity. The most

notable things are that the increase of inflow turbulence intensity increases horizontal velocity near the roof level (Fig. 9d) and downward motion at the roof level of the downwind region of the street canyon (Fig. 10d). The increased horizontal velocity strengthens vortex intensity and the increased downward motion allows for more incoming of turbulent eddies into the street canyon. When the inflow turbulence intensity is relatively weak, a relatively small amount of turbulent eddies stream into the street canyon across the roof level near the downwind building (Fig. 11a). In this case, the regions of downward motion and reversed flow are not largely extended owing to relatively weak eddy activity and its small effect on momentum redistribution in the street canyon. Therefore, because momentum transfer into the street canyon increases, the maximum horizontal and vertical velocities increase with increasing inflow turbulence intensity.

When the inflow turbulence intensity is relatively strong, a relatively large amount of turbulent eddies stream into the street canyon across the roof level near the downwind building (Fig. 11b). In this case, the regions of downward motion and reversed flow are largely extended owing to relatively strong eddy activity and its large effect on momentum redistribution by mixing momentum and decreasing velocity peaks in the street canyon. Therefore, despite the increase of momentum transfer into the street canyon, the maximum downward and reversed horizontal velocities decrease. There are two good examples for the momentum redistribution by the increase of turbulent diffusivity. The first is shown in Fig. 8c. Here, the maximum intensity of reversed horizontal velocity decreases but the reversed horizontal velocity strengthens at most locations in the lower layer. The second is shown in Figs. 10b and c. Here downward velocity strengthens at most locations despite the decrease of maximum downward velocity. These facts are indicated by bold arrows in Fig. 11b.

3.2. *Inflow turbulence intensity effects on pollutant dispersion*

Fig. 12 shows pollutant concentration fields at $t = 1$ h in the cases of TI20, TI40, TI60, and TI80. Note that the conservation equation for pollutants is integrated for 1 h using flow fields at $t = 1$ h. A similar distribution pattern appears in all the cases. Pollutants emitted at the street bottom are transported to the upwind region in the lower layer of the street canyon and then transported to the upper layer of the street canyon. Therefore, the maximum concentration at any height is observed in the upwind region. Once pollutants are transported to the upper layer, some of them escape from the street canyon and others are transported into the street canyon again. The concentration is low in the downwind region where air with relatively low pollutant concentration streams into the street canyon.

The residue concentration ratio is defined as the ratio of the total amount of pollutants remaining in the street canyon to the total amount of pollutants emitted during the integration. This ratio and the average concentration in the street canyon as a function of inflow turbulence intensity are plotted in Fig. 13. Both the residue concentration ratio and average concentration for a given time decrease with increasing inflow turbulence intensity. For a given inflow turbulence intensity, the

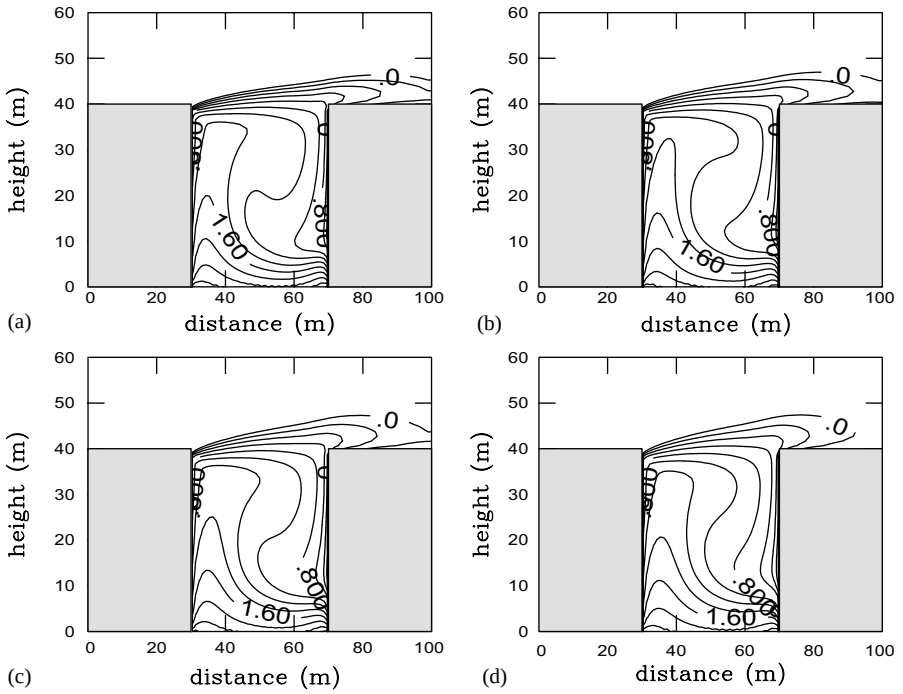

Fig. 12. Pollutant concentration (in ppb) fields at $t = 1$ h in the (a) TI20, (b) TI40, (c) TI60, and (d) TI80 cases. The values are on a log scale in base 10. The contour interval is 0.2.

residue concentration ratio decreases with time (Fig. 13a). For a given inflow turbulence intensity, the average concentration increases with time but becomes roughly constant after $t = 2700$ s (Fig. 13b). That is, it reaches a quasi-steady state in which the total amount of pollutants emitted is equal to the net total amount of pollutants escaping from the street canyon at any time. Pollutant concentration reaches a quasi-steady state earlier in the ST case than in the WT case.

Fig. 14 shows the time series of pollutant concentration at $z = 2$, 20, and 40 m of the street canyon center ($x = 50$ m) in the cases of TI20, TI40, TI60, and TI80. Note that the vertical scales are different from each other in these plots. At the lower layer (Fig. 14a), the concentration increases rapidly at the early stage of the time integration and reaches a quasi-steady state more quickly than that at other heights. At a quasi-steady state, the concentration becomes low as the inflow turbulence intensity increases. At $t = 30$ min, the pollutant concentration in the TI20 case is 1.5 times higher than that in the TI80 case. At the middle layer (Fig. 14b), the concentration becomes high as the inflow turbulence intensity increases at the early stage. However, after $t \sim 18$ min, the concentration becomes low with increasing inflow turbulence intensity. At the roof level (Fig. 14c), as the inflow turbulence intensity increases, the concentration at the early stage slightly becomes high but after $t \sim 8$ min, the concentration becomes low. It takes time for pollutants to be

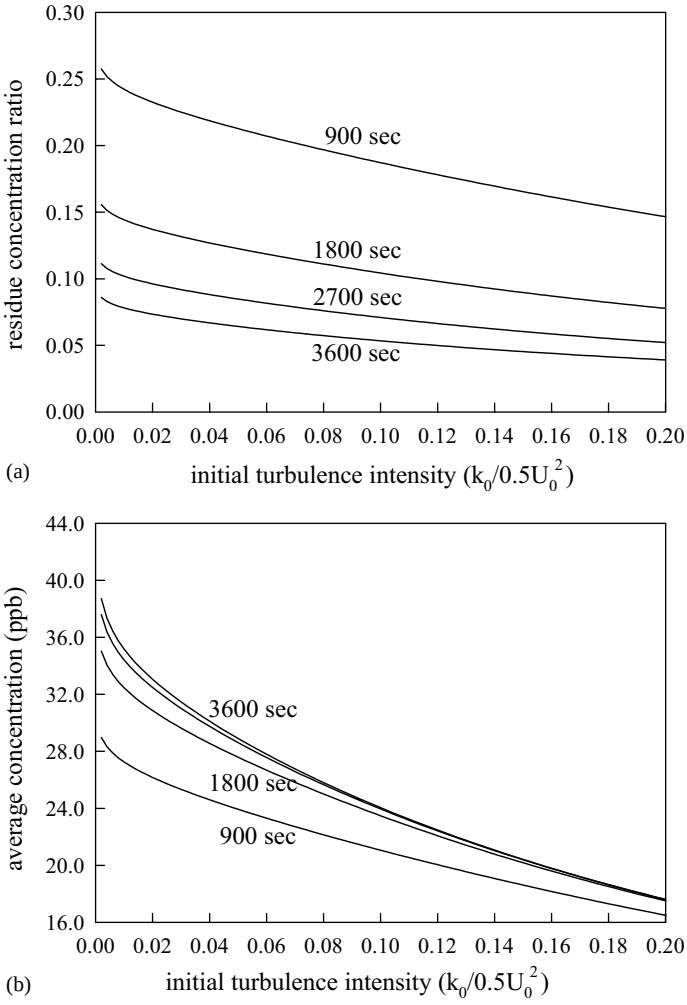

Fig. 13. (a) Residue concentration ratio and (b) average concentration in the street canyon at 900, 1800, 2700, and 3600 s as a function of inflow turbulence intensity.

transported from the source region at the street bottom to the roof level of the street canyon. As the inflow turbulence intensity increases, pollutant transport becomes fast not only because the upward velocity increases (Fig. 7a) but also because turbulent diffusivity increases (Fig. 6). Therefore, as the inflow turbulence intensity increases, the concentration at any height becomes high at the early stage but low eventually.

Fig. 15 shows the horizontal distributions of pollutant concentration at $z = 5$, 15, 25, and 35 m in the cases of TI20, TI40, TI60, and TI80. As the inflow turbulence intensity increases, the horizontal gradient of pollutant concentration decreases near

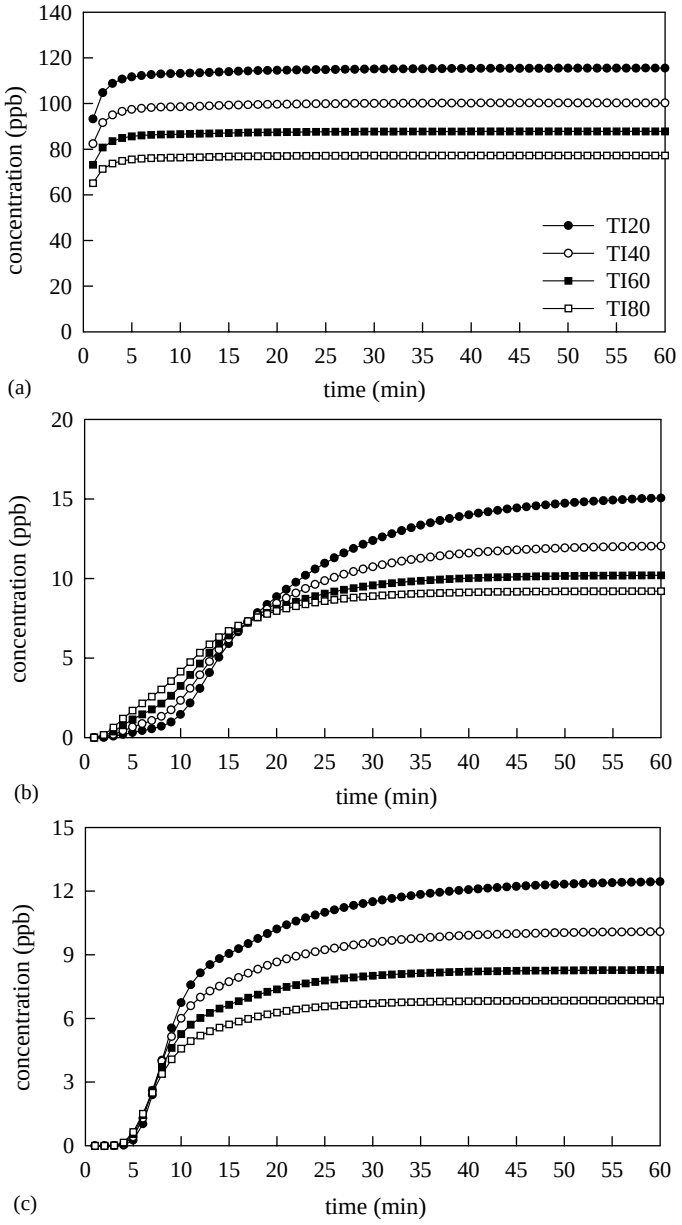

Fig. 14. The time series of pollutant concentration at (a) $z = 2$ m, (b) $z = 20$ m, and (c) $z = 40$ m of the street canyon center ($x = 50$ m) in the TI20, TI40, TI60, and TI80 cases.

the upwind and downwind buildings. At $z = 5$ m, local highs of pollutant concentration are observed in both the upwind and downwind regions. The reversed horizontal and downward velocities are very small near the downwind local high.

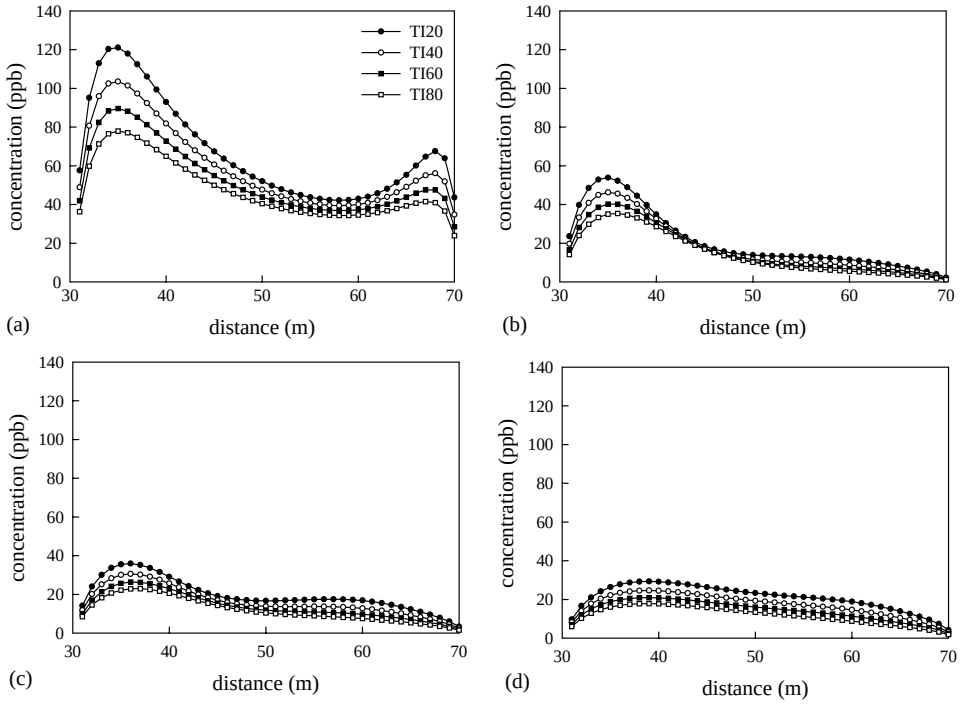

Fig. 15. The horizontal distributions of pollutant concentration at (a) $z = 5$ m, (b) $z = 15$ m, (c) $z = 25$ m, and (d) $z = 35$ m in the TI20, TI40, TI60, and TI80 cases.

The eddy diffusion and the advection by the upward motion of the small corner vortex near the downwind corner region rather than the advection by the reversed flow and downward motion of the main vortex play important roles in transporting pollutants upward. On the other hand, near the upwind local high, the advection and diffusion processes take place in the same direction. In this region, pollutants are transported upward by both the upward motion of the main vortex and the eddy diffusion. As a result, the maximum concentration is observed in the upwind region. At $z = 15$ m, the downwind local high is not observed any more. As mentioned above, the maximum reversed horizontal velocity is observed near $z = 15$ m. Pollutants transported from the lower layer by the eddy diffusion is transported to the upwind region by the reversed flow. This is responsible for eliminating the downwind local high. In the upwind region, pollutants are converged not only from the lower layer by the upward velocity and eddy diffusion but also from the center and downwind regions by the strong reversed flow.

At $z = 25$ m, the average horizontal gradient of pollutant concentration decreases in the upwind region ($\sim 30\,\text{m} < x < \sim 50\,\text{m}$) compared with that at $z = 15$ m. At $z = 35$ m, there is no distinct local high in the upwind region. At this height, pollutants are transported to the downwind region by the strong horizontal velocity.

As a result, the upwind local high disappears and the difference in concentration between the upwind and downwind region decreases compared with that in the lower layer. Above $z = 15$ m in the downwind region, the concentration in the upper layer is higher than that in the lower layer (Figs. 15b, c, and d). This is because some of pollutants transported to the upper layer in the upwind region stream again into the downwind region of the street canyon.

Figs. 13–15 indicate that the inflow turbulence intensity significantly affects pollutant concentration in the street canyon and pollutant escape from the street canyon.

4. Summary and conclusion

This study investigated the effects of inflow turbulence intensity on mean flow, turbulence, and pollutant dispersion in an urban street canyon with a street aspect ratio of 1. For this, numerical experiments with different inflow turbulence intensities were performed using a two-dimensional model. It was shown that as the inflow turbulence intensity increases, TKE and turbulent diffusivity in the street canyon increases. It was also shown that with increasing inflow turbulence intensity, the horizontal velocity near the roof level increases and the street-canyon vortex strengthens. The analyses of the time series and residue ratio of pollutant concentration indicated that the inflow turbulence intensity significantly influences pollutant concentration in the street canyon. It was shown that as the inflow turbulence intensity increases, the pollutant concentration in the street canyon becomes low and hence pollutant escape from the street canyon is facilitated.

In this study, a simple building-configuration in two dimensions was considered with specified inflow turbulence intensity at the inflow boundary in order to examine the effects of inflow turbulence intensity on flow and pollutant dispersion in an urban street canyon. The results presented in this basic study are expected to help understand inflow turbulence intensity effects in complex urban situations.

Acknowledgements

This research was supported by the Climate Environment System Research Center sponsored by the SRC Program of the Korea Science and Engineering Foundation. This research was also supported by the Brain Korea 21 Program.

Appendix A. Parameterization of turbulent processes

The turbulent diffusivity of momentum in the horizontal and vertical momentum equations and the turbulent diffusivity of pollutants in the transport equation for

pollutant concentration can be expressed as

$$K_m = C_\mu \frac{k^2}{\varepsilon}, \tag{A.1}$$

$$K_c = \frac{K_m}{Sc_t}, \tag{A.2}$$

respectively. Here, k and ε are the TKE and its dissipation rate, respectively, C_μ is an empirical constant, and Sc_t is the turbulent Schmidt number. In the present model, k and ε are prognostically computed using (a $k-\varepsilon$ turbulence closure model)

$$\frac{\partial k}{\partial t} + U\frac{\partial k}{\partial x} + W\frac{\partial k}{\partial z} = K_m\left\{2\left[\left(\frac{\partial U}{\partial x}\right)^2 + \left(\frac{\partial W}{\partial z}\right)^2\right] + \left(\frac{\partial U}{\partial z} + \frac{\partial W}{\partial x}\right)^2\right\} + \frac{\partial}{\partial x}\left(\frac{K_m}{\sigma_k}\frac{\partial k}{\partial x}\right) + \frac{\partial}{\partial z}\left(\frac{K_m}{\sigma_k}\frac{\partial k}{\partial z}\right) - \varepsilon, \tag{A.3}$$

$$\frac{\partial \varepsilon}{\partial t} + U\frac{\partial \varepsilon}{\partial x} + W\frac{\partial \varepsilon}{\partial z} = C_{\varepsilon 1}\frac{\varepsilon}{k}K_m\left\{2\left[\left(\frac{\partial U}{\partial x}\right)^2 + \left(\frac{\partial W}{\partial z}\right)^2\right] + \left(\frac{\partial U}{\partial z} + \frac{\partial W}{\partial x}\right)^2\right\} + \frac{\partial}{\partial x}\left(\frac{K_m}{\sigma_\varepsilon}\frac{\partial \varepsilon}{\partial x}\right) + \frac{\partial}{\partial z}\left(\frac{K_m}{\sigma_\varepsilon}\frac{\partial \varepsilon}{\partial z}\right) - C_{\varepsilon 2}\frac{k^2}{\varepsilon}, \tag{A.4}$$

where U is the mean horizontal velocity in the x direction, W the mean horizontal velocity in the z direction. $\sigma_k, \sigma_\varepsilon, C_{\varepsilon 1}$, and $C_{\varepsilon 2}$ are empirical constants. The constants in (A.1)–(A.4) are specified as

$$(C_\mu, \sigma_k, \sigma_\varepsilon, C_{\varepsilon 1}, C_{\varepsilon 2}, Sc_t) = (0.09, 1.0, 1.3, 1.44, 1.92, 0.9). \tag{A.5}$$

References

[1] F.T. DePaul, C.M. Sheih, Measurements of wind velocities in a street canyon, Atmos. Environ. 20 (1986) 455–459.
[2] J.-J. Baik, J.-J. Kim, A numerical study of flow and pollutant dispersion characteristics in urban street canyons, J. Appl. Meteorol. 38 (1999) 1576–1589.
[3] F.T. DePaul, C.M. Sheih, A tracer study of dispersion in an urban street canyon, Atmos. Environ. 19 (1985) 555–559.
[4] I.Y. Lee, H.M. Park, Parameterization of the pollutant transport and dispersion in urban street canyons, Atmos. Environ. 28 (1994) 2343–2349.
[5] B.J. Wedding, D.J. Lombardi, J.E. Cermak, A wind tunnel study of gaseous pollutants in city street canyons, J. Air Pollut. Control Ass. 27 (1977) 557–566.
[6] W.G. Hoydysh, W.F. Dabberdt, Kinematics and dispersion characteristics of flows in asymmetric street canyons, Atmos. Environ. 22 (1988) 2677–2689.
[7] W.F. Dabberdt, W.G. Hoydysh, Street canyon dispersion sensitivity to block shape and entrainment, Atmos. Environ. 25A (1991) 1143–1153.
[8] J.-J. Baik, R.-S. Park, H.-Y. Chun, J.-J. Kim, A laboratory model of urban street-canyon flows, J. Appl. Meteorol. 39 (2000) 1592–1600.
[9] K. Uehara, S. Murakami, S. Oikawa, S. Wakamatsu, Wind tunnel experiments on how thermal stratification affects flow in and above urban street canyon, Atmos. Environ. 34 (2000) 1553–1562.

[10] J.-J. Kim, J.-J. Baik, A numerical study of thermal effects on flow and pollutant dispersion in urban street canyons, J. Appl. Meteorol. 38 (1999) 1249–1261.
[11] J.-J. Kim, J.-J. Baik, Urban street-canyon flows with bottom heating, Atmos. Environ. 35 (2001) 3395–3404.
[12] P. Louka, S.E. Belcher, R.G. Harrison, Modified street canyon flow, J. Wind Eng. Ind. Aerodyn. 74–76 (1998) 485–493.
[13] N. Kato, T. Ohkuma, J.R. Kim, H. Marukawa, Y. Niihori, Full scale measurements of wind velocity in two urban areas using an ultrasonic anemometer, J. Wind Eng. Ind. Aerodyn. 41–44 (1992) 67–78.
[14] Y.Q. Zhang, A.H. Huber, S.P.S. Arya, W.H. Snyder, Numerical simulation to determine the effects of incident wind shear and turbulence level on the flow around a building, J. Wind Eng. Ind. Aerodyn. 46–47 (1993) 129–134.
[15] M.J. Brown, R.E. Lawson, Jr., D.S. DeCroix, R.L. Lee, Mean flow and turbulence measurements around a 2-D array of buildings in a wind tunnel, 11th Joint Conference on the Applications of Air Pollution Meteorology with A&WMA, American Meteorological Society, Long Beach, CA, 2000, pp. 35–40.
[16] W.S. Smith, J.M. Reisner, D.S. DeCroix, M.J. Brown, R.L. Lee, S.T. Chan, D.E. Stevens, A CFD model intercomparison and validation using high resolution wind tunnel data, 11th Joint Conference on the Applications of Air Pollution Meteorology with A&WMA, American Meteorological Society, Long Beach, CA, 2000, pp. 41–46.
[17] M.W. Rotach, Profiles of turbulence statistics in and above an urban street canyon, Atmos. Environ. 29 (1995) 1473–1486.
[18] J.-J. Baik, J.-J. Kim, On the escape of pollutants from urban street canyons, Atmos. Environ. 36 (2002) 527–536.